DETAILED ANALYSIS OF CLOUD SYSTEMS OBSERVED DURING TOGA-COARE: SIMULATIONS FORCED & UNFORCED BY THE LARGE SCALE MOTIONS

J.L.Redelsperger and F. Guichard

Centre National de Recherches Météorologiques
(Météo-France and CNRS)

1 INTRODUCTION

Accurate representation of cloudy processes in general circulation models is one of the most challenging problems of climate research and weather forecasting. The region of the Tropical Ocean Global Atmosphere Coupled Ocean-Atmosphere Response Experiment (TOGA-COARE) corresponds to a huge warm pool located in the western equatorial Pacific Ocean, and is so one of the most convectively active region on the planet. For this reason, the improvement of cloud parameterization is a major objective of TOGA-COARE. Two main datasets of TOGA-COARE relevant to this issue concern the large scale (from the sounding network) and the cloud scale (mainly from surface radars, airborne Doppler radars and aircrafts). Results presented in this paper are based on these datasets and simulations using a Cloud-Resolving Model (CRM). Two different approaches are used, corresponding to the development of convection unforced and forced respectively by large scale motions.

The first case concerns the development of convective lines, oriented approximately parallel to a moderate low level shear. Although these kinds of convective systems have not yet been intensively studied, they appeared to be very common during TOGA-COARE (Summary report of the TOGA-COARE International Data Workshop), over the Western Equatorial Pacific, where the wind shear is often weak. A characteristic of this system is the absence of large-scale ascent (as analyzed from the ECMWF fields) and of the complex interactions with other convective clouds. Hence this is a specific case where convection occurs without the presence of large-scale convergence. In such a case, convection schemes using a closure on the large scale convergence of moisture would fail to capture this convective event. Three-dimensional simulations using a cloud-resolving model on a large domain have been realized and compared to observations at cloud-scale. In this case, any large scale convergence is prescribed. More detailed results concerning this case are also reported in Guichard *et al.*(1996b).

The second case decribed in this paper concerns the period of 11-18 December 1992, corresponding to a well-marked transition of wind regimes over the experimental region: from light winds (1m/s) to a westerly wind burst. The period also corresponds to the development of active convective systems and to an observed large scale convergence. The numerical approach used for this case is to run the cloud-resolving model, forced by large scale advections and fluxes as deduced from the network of COARE experiment. This approach follows the one generally used to evaluate cloud parameterization using a single column model, except that the convection is explicitly resolved here. The presented results concern a two-dimensional 7-day simulation of convective systems forced through fields observed during this period (provided by P. Ciesielsky and R. Johnson, CSU) and computed radiative effects.

The main goal of present work is to use advanced diagnostics applied to CRM simulations, in order to provide new insights for development and evaluation of convective parameterizations in GCMs. The simulation domain is partitioned into internal areas, including convective and stratiform precipitation areas as well as shallow, anvil cloud areas and clear sky columns. Also convective and

stratiform region are also partioned in updraft and downdraft regions. The contributions of different internal areas to the total cloud ensemble impact are analysed, and complete budgets of main thermodynamical variables over these areas are discussed. Thus, from a complex cloud ensemble, we come to a simpler and more understandable system formally analogous to 1D cloud model type that are used in mass flux convection schemes.

The cloud-resolvind model, the partitioning method and the budget equations are presented in section 2. The first case of convective lines unforced by large scale motion is presented in section 3, whereas the second case of 7-day simulations forced by observed large scale motions is presented in section 4.

2 THE CLOUD-RESOLVING MODEL

2a General features

The three–dimensional cloud model is described in detail by Redelsperger and Sommeria (1981, 1986). The governing system is the primitive non-hydrostatic anelastic set of equations. The spatial discretization is of second order on an Arakawa type–C grid and it uses the leap–frog temporal scheme. A temporal filter (Asselin, 1972) and a fourth order horizontal diffusion operator (as described in Redelsperger and Lafore, 1988) are applied to the prognostic variables in order to damp short temporal and spatial oscillations, respectively. In all experiments, the vertical coordinate is stretched with a mesh interval measuring from 70 m near the ground to 1000 m above the tropopause.

Model prognostic variables are the three components of the wind, u, v and w, the potential temperature θ, the specific humidity q_v, specific contents for five hydrometeor species (cloud liquid droplets q_c, rain drops q_r, ice crystals q_i, aggregates q_n and graupel q_h) and the sub-grid turbulent kinetic energy e_t.

A Kessler-type parameterization is used for warm microphysical processes, except for sub-grid scale condensation and conversion from cloud droplets in rain drops (Redelsperger and Sommeria 1986). Ice phase microphysics is treated with the scheme developed by Caniaux *et al.*(1994).

The parameterization scheme for subgrid–scale turbulence is based on an assumption of zero third–order moments in the basic equations. The second–order moments are expressed as a function of the turbulent kinetic energy, which is given by a prognostic equation (Redelsperger and Sommeria, 1981; Balaji and Redelsperger, 1996). One advantage of this scheme is a correct description of anisotropic turbulent exchanges in stable layers, which is not the case with simpler formulations. A modification has been made to the scheme to distinguish the horizontal and vertical mixing length in the second–order momentum equations, as the horizontal mesh size is much larger than the vertical. The subgrid fluctuations of the thermodynamic variables are taken into account in the condensation and evaporation (C.E) scheme, to allow for partial condensation over grid volumes. In addition, the C.E scheme and the subgrid turbulent parameterization are formulated in terms of temperature and water variables which are conserved to a good approximation through C.E processes.

Radiative effects are computed fully interactively with the cloud field using the radiation scheme of the ECMWF (Morcrette 1991- see Guichard *et al.*1996a for its implementation in the CRM).

2b Partitioning the system into different areas

The cloud systems under study are typically a composite, including areas of intense convective activity as well as stratiform and clear sky regions. The global budgets, at the domain scale, are important, as they give the total impact of convection and the contribution of acting processes. Nevertheless, they only contain indirect information on what happens inside the domain. With a partition of the total domain into different internal areas, it is possible to get statistical information

on the cloud ensemble, such as the intensity of convective drafts or the relative contribution of stratiform areas.

An additional interest of the domain splitting is related to mass flux schemes of convection. In effect, theses parameterizations are based on a similar decomposition of the large-scale grid box. They assume that columns consist of restricted convective areas surrounded by a quiet environment, and make assumptions on the behaviour of this system (Arakawa and Schubert, 1974 - Tiedtke 1989)

Lipps and Hemler (1986) and Tao *et al.*(1987) have pursued such statistical analyses of simulated deep cloud ensembles, using a method of partitioning based on a distinction between clear and cloudy areas. For cloudy areas, they also differentiate updraft and downdrafts, and thus come to a detailed description of the cloud ensemble. Gregory and Miller (1989) and Krueger (1988) used a similar kind of partition. The decomposition of Gregory and Miller also included complex terms due to the fact that cloud area (σ_C) varies with height and in time. Our partition of the domain differs from these previous studies in that we define criteria distinguishing entire columns, and in that we considered a large number of internal areas (A_i).

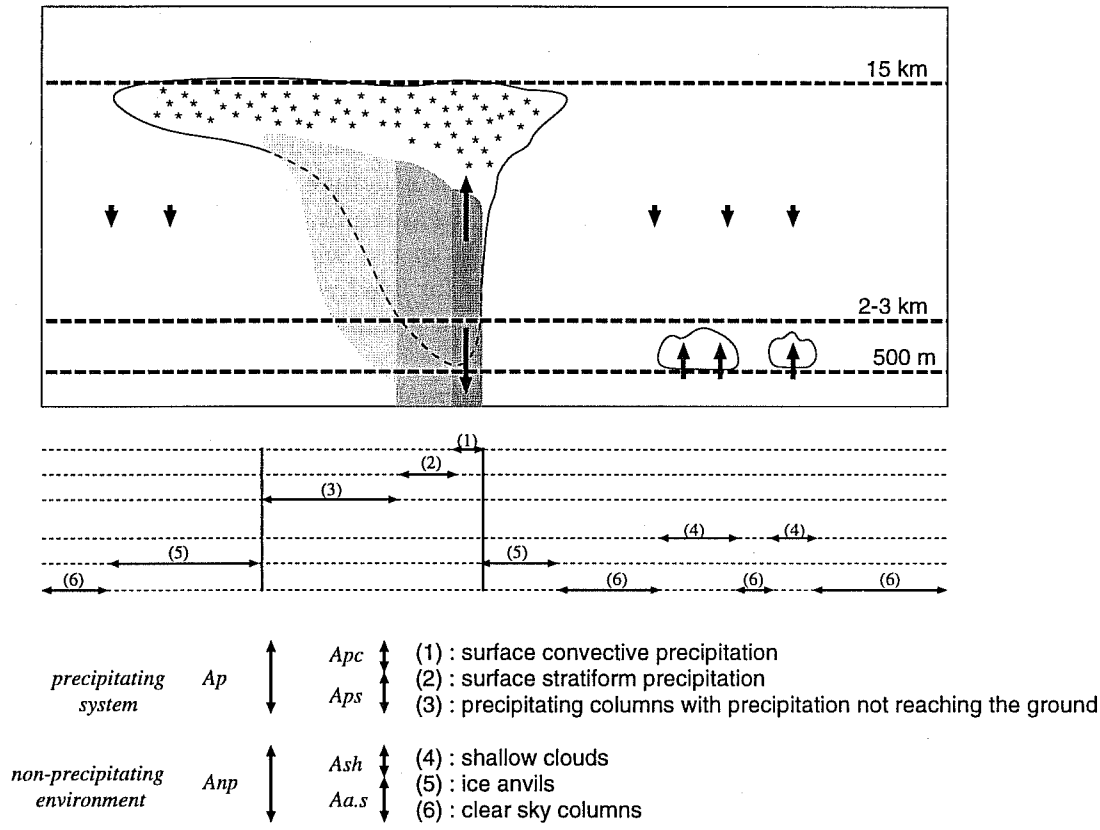

Figure 1: Schematic view of the cloud ensemble and its decomposition. (From Guichard *et al.*, 1996b)

Table 1 summarizes the criteria used to define 6 basic internal areas. We thus distinguish regions with convective precipitation A_1 (A_{p_c}), or stratiform surface precipitation A_2, trailing precipitation A_3, shallow clouds A_4 (A_{sh}), icy anvils A_5 or clear sky A_6 columns, as illustrated by Fig. 1.

Following Tao *et al.* (1989), the convective precipitation area A_{p_c} is defined as the ensemble of columns satisfying one of the two conditions: surface rainfall rate is greater than 20 mm h^{-1} or greater than 4 mm h^{-1} and twice as large as the average value taken over the 24 surrounding grid points, in this last case, the 8 closer surrounding columns are also retained as part of A_{p_c}. The shallow convection area A_{sh} definition is based on Sui *et al.* (1994). Each internal areas can be further split into updraft and downdraft sub-ensembles, so that up to 12 internal areas can be considered for some applications. The above criteria are applied at each model time step.

Table 1: Criteria used to define at each model time step the 6 basic internal areas. R is the surface precipitation and $IP = \int_0^H \rho(q_r + q_n + q_h)dz$ is the vertical integrated precipitating hydrometeor content. A_T corresponds to the total domain so that; $A_T = A_p + A_{np} = \sum_{i=1}^{6} A_i$. We also define intermediate areas; $A_{pc} = A_1$, $A_{ps} = A_2 + A_3$, $A_{sh} = A_4$ and $A_{a.s} = A_5 + A_6$.

Internal areas A_i			name	criteria	references
A_p precipitating system	A_{p_c}	A_1	convective areas	$R \geq 20$ mm h^{-1} or local maximum $R \geq 4$ mm h^{-1}	Tao *et al.* (1989)
	A_{p_s}	A_2	stratiform areas	$R \geq 0.5$ mm h^{-1}	
		A_3	trailing areas	$IP \geq 1$ kg m^{-2}	
A_{np} non-precipitating environment	A_{sh}	A_4	shallow clouds	$q_c + q_r + q_n + q_h \geq 5.10^{-6}$ kg kg^{-1}	Sui *et al.* (1994)
	$A_{a.s}$	A_5	icy anvils	$q_c + q_r + q_n + q_h + q_i \geq 5.10^{-6}$ kg kg^{-1} and no shallow clouds	
		A_6	clear sky colums		

2c Budget equations

Equations of evolution of θ and q_v of cloud-resolving model are expressed by:

$$\frac{\partial \theta}{\partial t} = -\frac{1}{\rho_0}\frac{\partial}{\partial x_j}\rho_0 \theta u_j + D_\theta + \frac{1}{\pi_0}Q^* + \frac{1}{\pi_0}Q_R + \left(\frac{\partial \theta}{\partial t}\right)_{LS} \quad (1)$$

$$\frac{\partial q_v}{\partial t} = -\frac{1}{\rho_0}\frac{\partial}{\partial x_j}\rho_0 q_v u_j + D_{q_v} - \frac{c_p}{L_v}Q + \left(\frac{\partial q_v}{\partial t}\right)_{LS} \quad (2)$$

In these equations, ρ is the density, L_v the latent heating horizontally averaged on the simulation domain, $\pi = T/\theta$ the Exner function, D_θ and D_{q_v} are the subgrid-scale diffusions; subscript 0 referes the anelastic base state only depending on height. Q_R is the net radiative heating rate (solar and infrared), Q^* the total latent heat release, including condensation, sublimation and fusion, whereas Q refers only to vapour heat release (i.e. condensation and sublimation). The difference between terms Q^* and Q is generaOlly weak and corresponds to the ice phase contribution through net fusion. Subcript LS refers to large scale advection. This forcing term vanishes in the first case (section 3), as large-scale convergence was found to be negligible, whereas it is prescribed from observations in the second case (section 4).

Thermodynamic variables θ and q_v will be horizontally averaged over internal areas A_i defined during the time interval $[t_1, t_2]$. The average of a quantity α over A_i is written:

$$\overline{\alpha}^i(z) = \frac{1}{\int_{t_1}^{t_2}\iint_{S_i} dsdt}\int_{t_1}^{t_2}\iint_{S_i}\alpha(z)\,dsdt$$

where S_i is the horizontal surface of the subdomain A_i at time t. For the particular case where the subdomain is defined as the whole simulation domain, the average will be written as $\overline{\alpha}^T$. The application of this operator results in the following budget equations expressed in terms of sensible heat source and latent heat sink:

$$\pi_0\overline{\frac{\partial \theta}{\partial t}}^i - \pi_0\left(\frac{\partial \theta}{\partial t}\right)_{LS} = -\pi_0\overline{\frac{\partial}{\partial x}u\theta}^i - \pi_0\overline{\frac{\partial}{\partial y}v\theta}^i - \frac{\pi_0}{\rho_0}\overline{\frac{\partial}{\partial z}\rho_0 w\theta}^i + \pi_0\overline{D_\theta}^i + \overline{Q^*}^i + \overline{Q_R}^i \quad (3)$$

$$-\frac{L_v}{c_p}\overline{\frac{\partial q_v}{\partial t}}^i + \frac{L_v}{c_p}\left(\frac{\partial q_v}{\partial t}\right)_{LS} = \frac{L_v}{c_p}\overline{\frac{\partial}{\partial x}uq_v}^i + \frac{L_v}{c_p}\overline{\frac{\partial}{\partial y}vq_v}^i + \frac{L_v}{c_p\rho_0}\overline{\frac{\partial}{\partial z}\rho_0 w q_v}^i - \frac{L_v}{c_p}\overline{D_{q_v}}^i + \overline{Q}^i \quad (4)$$

where the total transport has been split (first two *r.h.s.* terms of Eqs. 3 and 4) into horizontal and vertical terms. The contribution of each internal area A_i to the budget at the domain scale A_T is proportionnal to its average occupation rate σ_i:

$$\sigma_i = \frac{\int_{t_1}^{t_2}\iint_{S_i} ds dt}{(t_2 - t_1)\, S_T}$$

where S_T is the surface of the simulation domain. The budget equations at the whole domain scale become:

$$\pi_0\overline{\frac{\partial\theta}{\partial t}}^T - \pi_0\left(\frac{\partial\theta}{\partial t}\right)_{LS} = -\frac{\pi_0}{\rho_0}\overline{\frac{\partial}{\partial z}\rho_0 w\theta}^T + \overline{D_{Q_1}}^T + \overline{Q^*}^T + \overline{Q_R}^T \equiv Q_1 \quad (5)$$

$$-\frac{L_v}{c_p}\overline{\frac{\partial q_v}{\partial t}}^T + \frac{L_v}{c_p}\left(\frac{\partial q_v}{\partial t}\right)_{LS} = \frac{L_v}{c_p\rho_0}\overline{\frac{\partial}{\partial z}\rho_0 w q_v}^T + \overline{D_{Q_2}}^T + \overline{Q}^T \equiv Q_2 \quad (6)$$

which correspond to the apparent heat source Q_1 and apparent moisture sink Q_2 at the A_T scale (or domain scale). Horizontal fluxes vanish at the domain scale are commonly neglected in mass flux convection schemes.

3 CONVECTION UNFORCED BY LARGE SCALE MOTIONS

The thermodynamical impact of a cloud system, observed on 17 February 1993 in the Western Equatorial Pacific during TOGA-COARE, has been investigated with a cloud resolving model. This case study corresponds to the development during the night of convective lines, oriented approximately parallel to a moderate low level shear. This type of system is very common over the Western Equatorial Pacific, and is characterized by the absence of large-scale ascent. A more complete description of observations can be found in Jabouille *et al.* (1996) whereas a complete description of thermodynamical analysis is given in Guichard *et al.* (1996b). Two isolated parallel lines develop from clear sky conditions during the second part of the night, with a life cycle of the order of a few hours. Their length reaches 100-200 km in their mature stage and they lie approximately parallel to the low level shear. The conditions of simulation are similar to Jabouille *et al.* (1996) except for the inclusion of ice phase microphysics. The model is used with cyclic lateral boundary conditions, and starts at 22 h (local time) from horizontally homogeneous profiles derived from a radio-sounding. It must be noted that no large-scale advection is introduced for this case. Thus, external forcing consists only of surface heat fluxes and radiation. The model develops convection by itself starting from small random perturbations of temperature, thus avoiding an artificial initialization by a cold or warm perturbation often used.

The simulation is performed in 3D on a total domain of 90 by 90 km^2 in the horizontal and 20 km in height. The horizontal grid spacing is 900 m. The vertical grid is stretched, from 70 m resolution in the lower layers up to 700 m above 10 km. A time step of 10 s seconds is used and the model integration is done for 10 hours of physical time.

The three-dimensional simulation develops convection by itself, starting from small random perturbations of temperature, thus avoiding the artificial initialization by a cold or warm perturbation commonly used. A cloud population is simulated, including different types of clouds (shallow to deep), over 10h of its life cycle (Fig. 2). During a first stage dry rolls organize (STG0 on Fig.

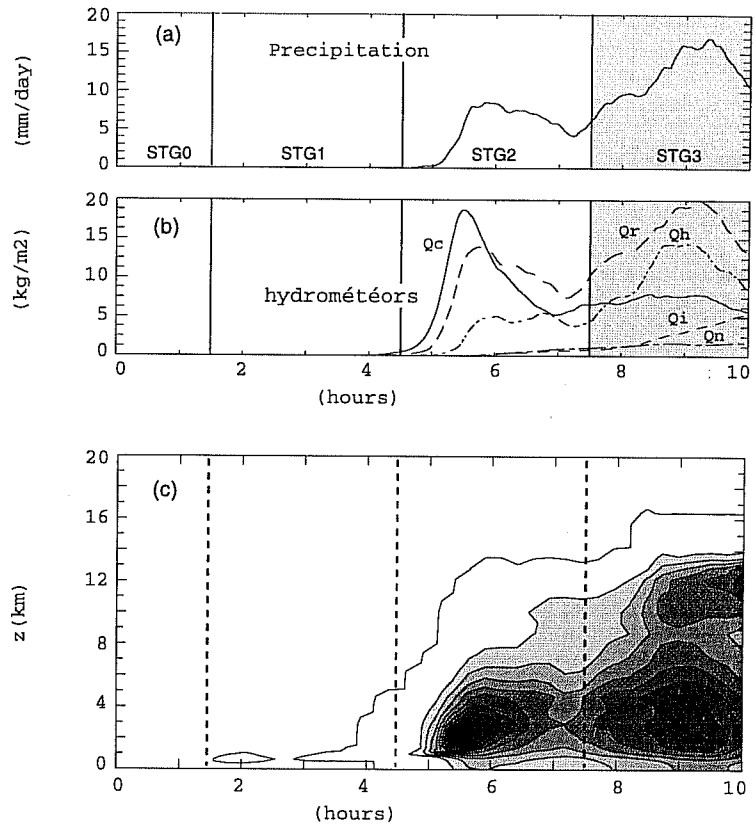

Figure 2: Time history of (a) precipitation in mm day^{-1}, (b) domain integrated water contents for each hydrometeor species in kg m^{-3}. and time sequence of (c) the total hydrometeor field $q_c + q_r + q_i + q_n + q_h$ averaged at the domain scale in kg kg^{-1}, the contour interval is 10^{-5}kg.kg−1. (From Guichard *et al.*, 1996bb)

2) and then small cumuli appear at the top of the boundary layer, but without generating precipitation (STG1). This stage is crucial to store humidity in the PBL, so that the following stage STG2 is explosive. It corresponds to the suddent release of the energy, through numerous convective clouds. Convection is mainly warm and cannot penetrate higher than 8 km, but is very efficient at moistening the 1.5-5 km layer. The last convective stage STG3 is the most intense, concerns the whole troposphere depth, and develops convective lines parallel to the low level shear and generates icy anvils. At the same time, shallow clouds also develop forced by lifting induced by convective subsidences.

The latent heat release $\overline{Q^*}^T$ (Fig. 3a) is responsible for a heating of the troposphere above 1 km and up to 12 km, reaching a maximum value of 7 K.s^{-1}. Its profile exhibits some classical features such as a strong cooling below 1 km caused by raindrop evaporation (Lafore *et al.*1988), a local minima below the height of the 0°C isotherm associated with solid hydrometeor melting (Caniaux *et al.* 1994). The major contribution to $\overline{Q^*}^T$ comes from the A_p, first from the convective area A_{p_c}, but also from the weaker precipitating zones A_{p_s} at higher and lower levels (Fig. 3b). Nevertheless as already found by Gregory and Miller (1989) latent heat released by shallow clouds (the A_{np} curve in Fig. 3a) can not be neglected. These clouds are responsible for intense condensation heating in a 1 km deep layer and for large cloud droplet evaporative cooling above. A comparison of vertical mass fluxes (not shown) and latent heat release (Fig. 3b) for the different internal areas shows a strong correlation between these two fields. As for mass fluxes, the convective precipitating area (covering a few percent of the domain) is responsible for the major part of the latent heat release occuring in A_p (Fig. 3b).

An analysis of potential temperature deviations for the different areas of cloud ensemble (not

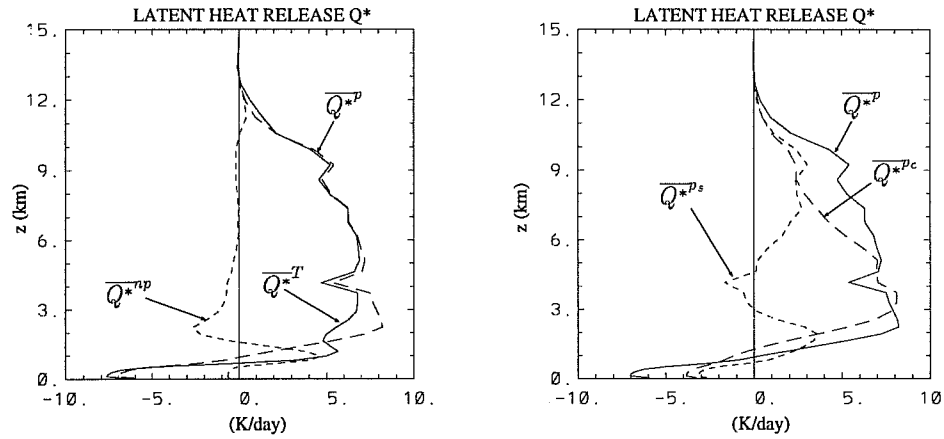

Figure 3: Vertical profiles of latent heat release for different areas ($\sigma_i \overline{Q^*}^i$) over [8h,10h] (a) for the total domain (A_T), precipitating system (A_p) and the non-precipitating environment (A_{np}), (b) same as (a) for the precipitating system (A_p) and its convective (A_{p_c}) and stratiform (A_{p_s}) parts. (From Guichard *et al.*, 1996b)

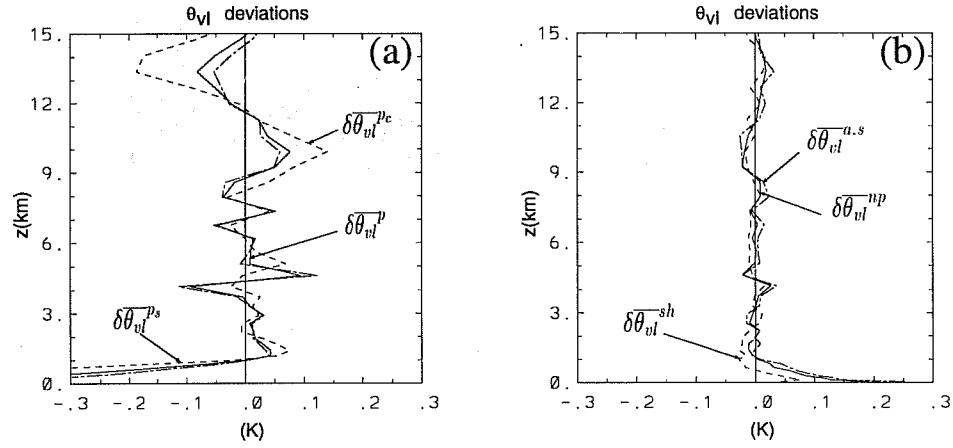

Figure 4: (a) and (b): Vertical profiles of deviations of liquid virtual potential temperature (in K) averaged over [8h,10h] (a) for the precipitating system (A_p), its convective (A_{p_c}) and stratiform (A_{p_s}) parts and (b) for the non-precipitating environment (A_{np}), the shallow clouds area included in it (A_{sh}) and the remaining anvil plus clear sky columns ($A_{a.s}$). (From Guichard *et al.*, 1996b)

shown) shows that the convective precipitation area is only slightly warmer than the other parts of the system, in agreement with previous aircraft data analysis (Jorgensen *et al.*1989, Lucas *et al.*1994). A good estimation of buoyancy is given by the deviations of liquid and solid virtual potential temperature θ_{vl} defined by: $\theta_{vl} = \theta\,(1 + \epsilon q_v - \sum q_\gamma)$, with $\sum q_\gamma$ the sum of the hydrometeor specific mixing ratios. Liquid and solid water virtual potential temperature deviations (Fig. 4) are weaker than potential temperature deviations, which mean that the excess buoyancy in clouds is extremely small. Buoyancy excesses that are necessary to generate convective clouds must therefore occur in very small and localized areas and at short time scales. In average, the system develops under a density equilibrium condition, involving both thermodynamics and microphysics through hydrometeor loading. The density equilibrium shows the speed and efficiency of the convection in modifying the environment through compensating subsidence and adjustment by internal gravity waves. In practice, an important consequence of this result is a relationship between thermodynamics and microphysics in and outside clouds, that could be useful for a convection scheme. Temperature deviations are also completely decoupled from vertical velocity fields, contrary to water vapour deviations which are positive in updraft layers and negative in downdraft layers.

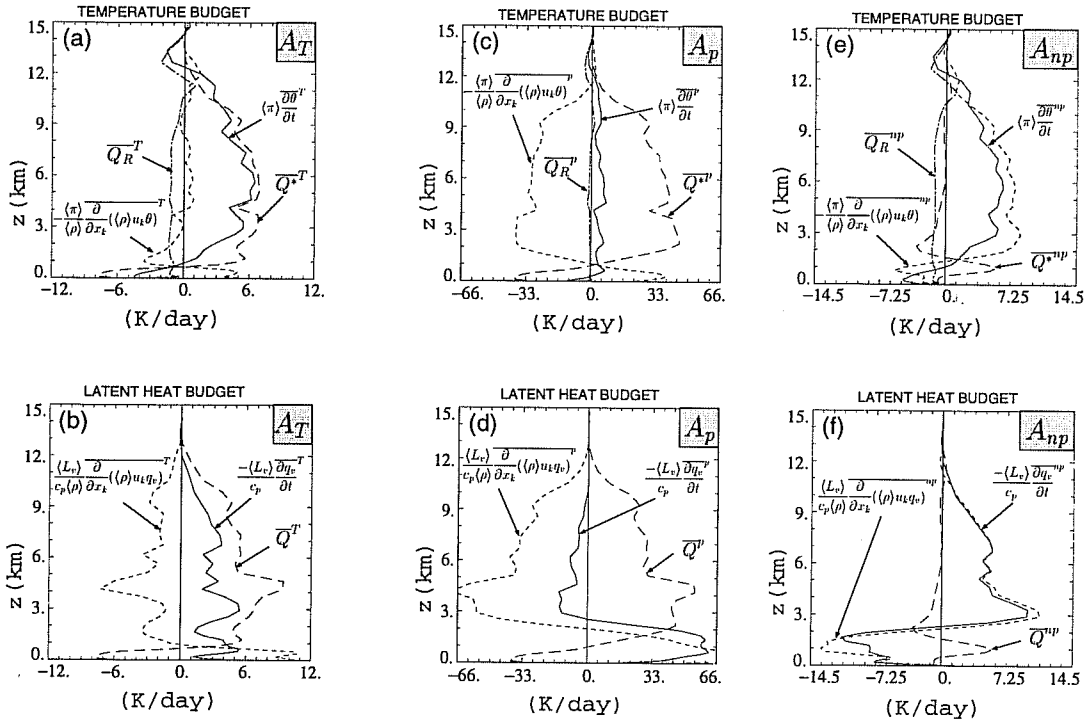

Figure 5: Budgets of temperature (a) and (b) horizontally averaged over the whole domain A_T and temporally over [8h,10h]; (b) and (c) same as (a) and (b) except for the precipitating area A_p; (d) and (e) same as (a) and (b) except for the non-precipitating area A_{np} non-precipitating area A_{np} - The horizontal scale is such that, multiplied by the rate of occupation (σ_p or σ_{np}) of the considered area, it gives the contribution of each area to the total budgets over A_T with the same horizontal scale. (From Guichard *et al.*, 1996b)

The thermodynamical impact of the system have been analysed in partitioning the total domain in internal areas as described in section 2, including convective and stratiform precipitating areas as well as clear sky columns. In the present case, without any large-scale advection, the budget equations of heat source and of moisture sink for the whole domain (Eqs. 5 and 6) correspond directly to the apparent heat source Q_1 and apparent moisture sink Q_2. Above the lowest kilometer, the system heats and dries during the deep convection stage STG3, but profiles of Q_1 and Q_2 are quite distinct (Fig 5a and b). This is now a classical feature that has often been highlighted for many convective systems, both from observations (Yanai *et al.* 1973, Johnson 1984) and modelling studies (Tao *et al.* 1986, Lafore *et al.*1988, Gregory and Miller 1989, Caniaux *et al.* 1994). The profile of Q_1 shows a maximum heating of about 6 K.day^{-1} located around 5-6 km, in agreement with profiles of Lin and Johnson (1996) over the TOGA-COARE region. The heating is mainly due to the latent heat release $\overline{Q^*}^T$. The sharp minimum at 4 km corresponds to melting occuring below the height of the 0°C isotherm. Convective transports are significant mainly below 2 km where they tend to reduce the subcloud evaporation of precipitating droplets and the net condensation between 1 and 2 km. We can see the radiative impact of high level anvil clouds, with a cloud top cooling around 12-13 km and a cloud base warming at 11 km. The profile of Q_2 is more complex, it shows several minima and maxima. In particular, we can see two maxima of Q_2 around 3-4 km and 9 km. Nevertheless, there is also a maximum located at the top of the subcloud layer ($\sim$ 1 km). As found by previous modelling studies (Lafore *et al.* 1988, Caniaux *et al.* 1994), differences in Q_1 and Q_2 profiles result in the main from differences in convective vertical transports of temperature and water vapour.

The decomposition of thermodynamical budgets (Figs. 5c to 5f) highlights the mechanisms of compensation occuring between the precipitating system and its environment. For temperature,

the latent heat release in the precipitating part is approximately compensated by the mean vertical advection, so that the contribution of this area to the total warming is small (Fig. 5c). The total warming occurs mainly in the environment, through compensating subsidence (Fig. 5e). Thus, to first order, the domain average temporal evolution of temperature can be explained by transports occurring in the environment, as suggested by Gregory and Miller (1989). The precipitating system is approximately in equilibrium as is assumed by some convection schemes (Arakawa and Schubert 1974, Tiedtke 1989). Moisture budgets are more complex to analyse (Figs. 5d and 5f). In the precipitating area (Fig. 5d), above 3 km, $\overline{Q^p}$ and transport approximately balance, resulting in a net moistening. Below 3 km, a strong drying can be found, associated with transports in downdrafts. In the environment, transports are the major processes and explain drying above 3 km as well as strong moistening below. Finally, below 3 km, the net domain drying appears as the result of stronger drying in the precipitating system A_p than moistening in the non precipitating environment A_{np}. Above 3 km, the opposite is found, as drying in the environment A_{np} dominates over moistening in the precipitating system A_p.

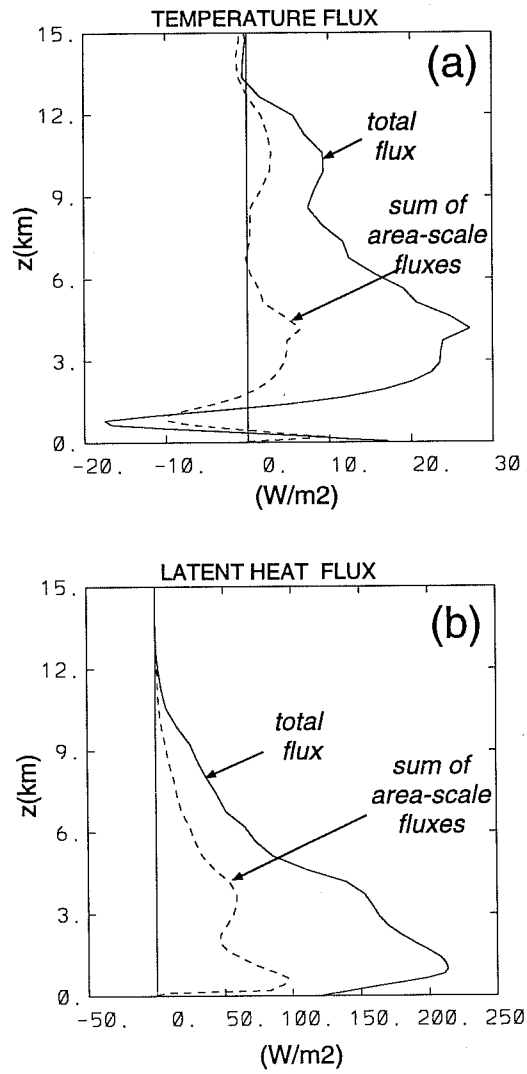

Figure 6: Sensible (a) and latent heat (b) fluxes: total fluxes $c_p \pi_0 \rho_0 \overline{w\theta}^T$ and $L_v \rho_0 \overline{wq_v}^T$ (solid lines curves) and contributions of area-scale fluxes (twelve different areas are retained here, see text)- curves correspond to a temporal average over [8h,10h]. (From Guichard *et al.*, 1996b)

Detailed analysis of sensible and latent heat vertical fluxes $c_p \pi_0 \rho_0 \overline{w\theta}^T$ and $L_v \rho_0 \overline{wq_v}^T$ have been

also performed. The structure of the temperature flux (Fig. 6a) shows many similarities with the ones simulated and observed by Sommeria and LeMone (1978) - hereafter SL78 - for trade wind shallow clouds. Firstly, the flux linearly decreases from the ocean surface (17 $W.m^{-2}$ here) to the top of the mixed layer (800 m). The minimum value (-18 $W.m^{-2}$) greatly increases up to more than -5 $W.m^{-2}$ in considering fluxes of virtual potential temperature. Above 800 m, the flux increases up to 25 $W.m^{-2}$ at 4 km, and decreases above except at 10 km where a second local maximum is present, related to high level cloud activity. This signature is similar to the one obtained by SL78, except that here the upward flux concerns all the deep convection layer up to 12 km, whereas flux stopped at 1400 m for the shallow clouds layer of SL78. Values of latent heat flux both at the surface and its vertical fluctuations are much more intense than those for temperature (Fig. 6b). It increases from 130 $W.m^{-2}$ at the surface up to 215 $W.m^{-2}$ at 1 km, bringing water vapour from this layer up to the free troposphere, where the flux gradually decreases. Above 12 km, the flux becomes negligible. For the convective stage STG3 here considered, it clearly appears that humidity previously stored below 1 km (stage STG1 in particular), is now upwardly transported. The importance of vapour transport is once again stressed by these profiles.

Any vertical flux on domain scale can be split on internal areas A_i as follow:

$$\rho_0 \overline{\alpha w}^T = \sum_i \rho_0 \sigma_i \overline{w}^i \left(\overline{\alpha}^i - \overline{\alpha}^T \right) + \sum_i \rho_0 \sigma_i \overline{w'_i \alpha'_i}^i$$

where $\sum_i$ corresponds to the sum on all internal areas A_i, and primes denote deviations from the average on internal area.

With this decomposition, the contributions of area-scale fluxes (the first term of the l.h.s.) and sub-area-scale fluxes (second term of the l.h.s.) can be determined. For some parameterization schemes only two internal areas are considered (cloud and environment). Here, we consider an ensemble of 12 distinct areas corresponding to the updrafts and downdrafts parts of the 6 basic internal areas defined in section 2. However, even with this fine scale decomposition of the domain, the sum of the area-scale fluxes (Fig. 6, dashed lines) explains only 1/3 to 1/2 of total flux. Decomposition with only the 6 basic internal areas degrades the estimation of the total flux (1/6 to 1/4).

Hence convective fluxes occur for a significant part on a very small scale, so that average draft profiles of vertical velocity, temperature and humidity are not adapted for their estimation. This result agrees with observations of convective clouds discussed in Emanuel (1991): they "reveal an extraordinary degree of inhomogeneity, with much of the vertical transport accomplished by subcloud-scale drafts". This is however the usual hypothesis for convection scheme using bulk convective drafts, together with relatively high temperature and water vapour deviations. Our results suggest that a suitable way to express convective transport in a bulk cloud model would be to take into account subdraft scale transports. It raises a closure problem as relations still need to be estimated between area-scale characteristics and sub-area-scale fluxes.

4 CONVECTION FORCED BY LARGE SCALE MOTIONS

We approach here the problem in using a cloud-resolving model, forced by large scale advections and fluxes as deduced from the network of COARE experiment. This approach follows the one generally used to evaluate cloud parameterization, except that the convection is explicitly resolved here. The present paper describes preliminary results of two-dimensional 7-day integration of convective systems forced through observed large-scale advective effects of heat and moisture and surfaces fluxes (provided by P. Ciesielsky and R. Johnson, CSU) and computed radiative effects. To force the model, a similar technique to Grabowski *et al.*(1996) is used. Time-evolving large scale wind field and time-evolving large scale advective tendencies of temperature and humidity are introduced in the cloud-resolving model. Observed surface fluxes are also used and keep horizontally constant in the model for this preliminary test.

The period selected for the present paper is 11-18 December 1992 and corresponds to a well-marked transition in wind regime over the experimental region: from light winds (1m/s) to a westerly wind burst (not shown). As illustrated by the evolution of observed and simulated surface rainfall (Fig. 7), 3 major convective events occur during this period,with a peak around 50 mm/day (6-hour mean) for the first convective event.

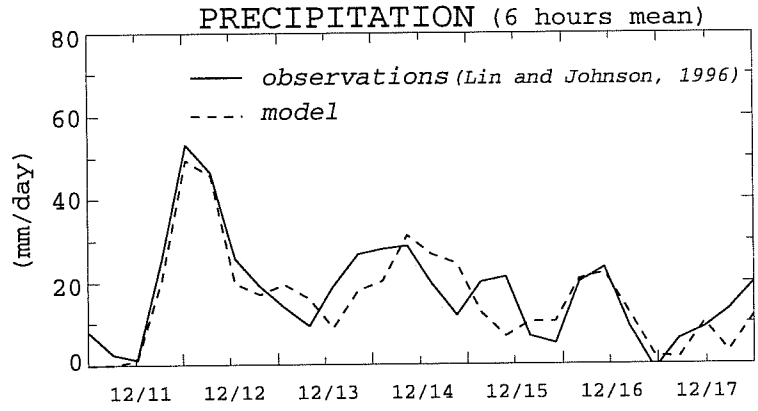

Figure 7: Evolution of the domain-averaged 6-h mean of the surface rainfall as estimated from moisture budget (continue line) by Lin and Johnson (1996) and present simulation (dashed line).

The convective and stratiform precipitation area occupancies as deduced from simulations (Fig. 8) indicate that the convective area (see definition in section 2) is always very restricted, covering less than 5% of the total domain. The stratiform precipitation region is more varying with peaks of occupancies around 25%.

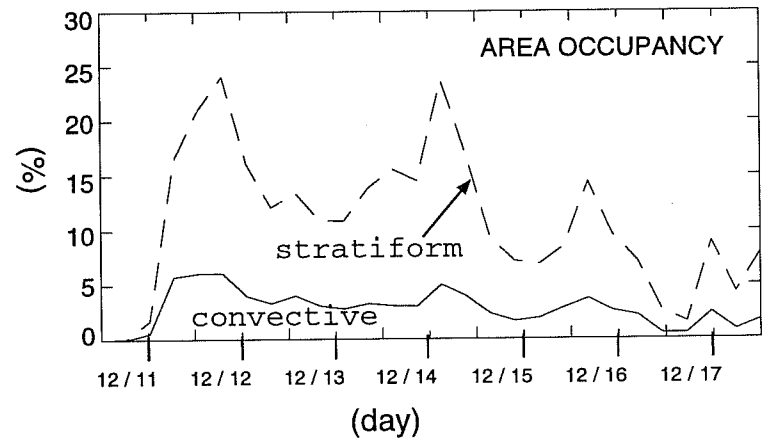

Figure 8: Evolution of convective and stratiform area occupancies as simulated.

To each 3 major convective events correspond a strong cooling and drying in the middle troposphere, as shown by the observed evolution of the apparent heat source Q_1 and the apparent moisture sink Q_2 (Figs. 9a and 9b). The maximum of Q_1 and Q_2 is 20 and 16 K/day, respectively. The model reproduces well these systems and the agreement between the observed and simulated Q_1 and Q_2 behaviour is quite satisfactory (Figs. 9c and 9d). The largest difference (+/- 3K/day) between observed and model-produced Q_1 source occurs in the upper troposphere (above 12 km). In this region, the model seems to overestimate and to underestimate the source Q_1 during suppressed and active convection period, respectively. In contrast, the largest differences for the Q_2 sink (same value than for Q_1 except in small spots) occur in the lower troposphere (below 6 km). Differences

seem related to a time-shift between the model and observations, with succession of minima and maxima (Figs. 9e and 9f).

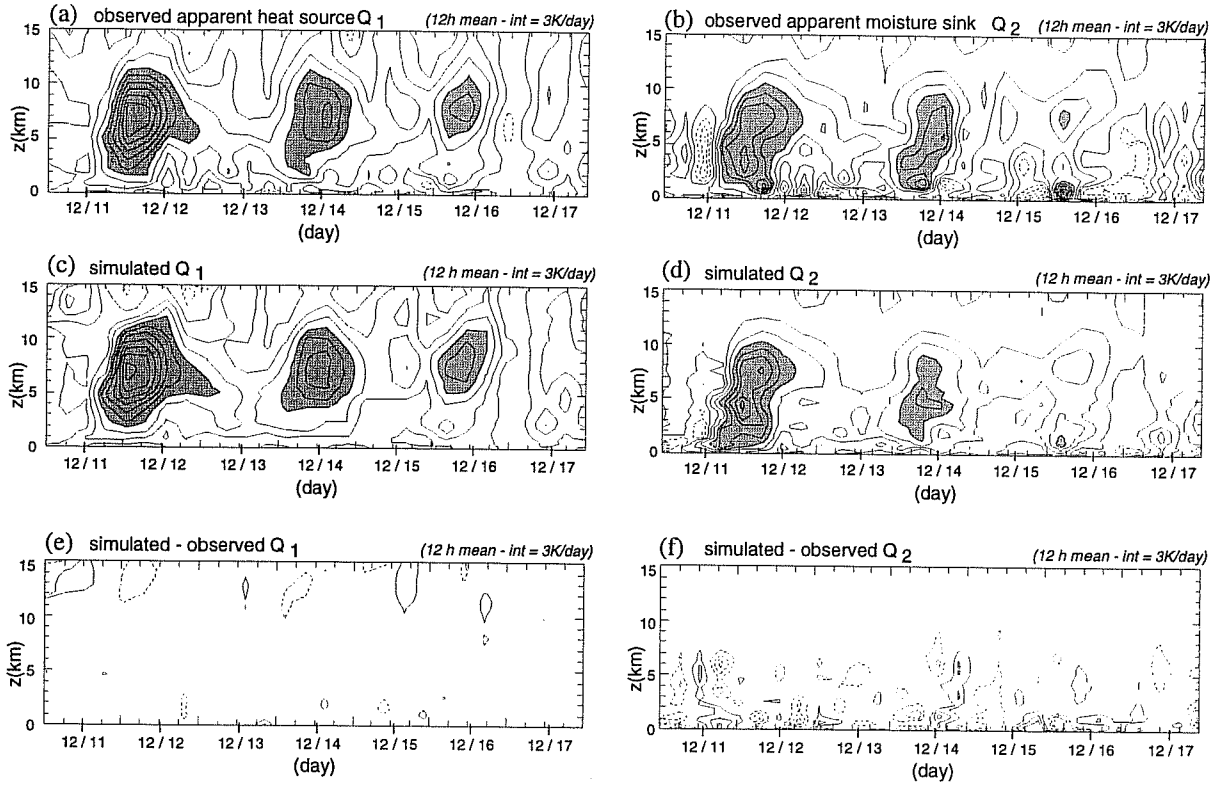

Figure 9: Evolution of the domain-averaged 12-h mean observed apparent heat source Q_1 (a) and apparent moisture sink Q_2 (b), simulated Q_1 (c) and Q_2 (d), and differences between simulated and observed Q_1 (e) and Q_2 (f) - contour interval is 3 K day^{-1}.

These results are confirmed in considering the average over the 7 day period (Figs. 10a and 10b). The agreement for Q_1 is good except that the model predicts Q_1 values larger and smaller (.5 K/day) than observed, between 11 and 13 km and above 13 km respectively. For Q_2, a difference less than 1K/day is found in the lower troposphere (up to 8 km).

Comparison of differences between observed and modeled domain-average profiles of temperature and vapor mixing ratio (not shown) indicates that the simulated temperature is too cold (1 K) in the lower and middle troposphere for the first convective event (12 December). In the upper troposphere, the model seems to overestimate the temperature (2-3 K) during periods just preceding the convective ones and during the convection initiation phase. Significant differences in the first 5km are found in the humidity field and can be related to the surface fluxes used for this first test (see above). The difference is indeed increasing with the time and seems to come from the boundary layer.

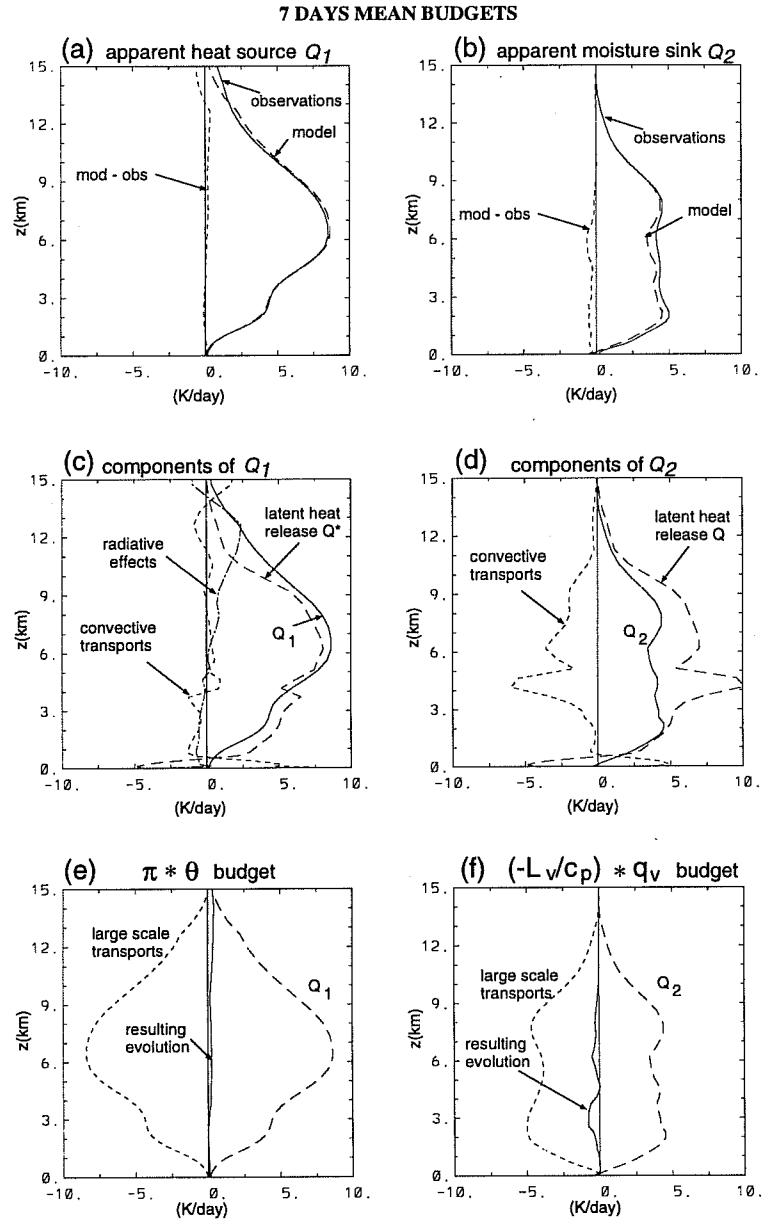

Figure 10: 7 days mean observed and simulated Q_1 (a) and Q_2 (b); contributions to profiles of the model-produced Q_1 (c and e) and Q_2 (d and f).

Though the results of simulations in term of large scale impact show some differences with the results deduced from observations, they are considered enough good to use them to analyze in details the cloud systems as did in section 3 for the 17 Feb 1993 case. Looking at the 7-day average of the partioning of Q_1 and Q_2 (Figs. 10c and 10d) in eddy transports and latent heat release indicate similar results than those described in section 3 for the unforced case. The main feature is the importance of vertical transport larger for vapor than for temperature.

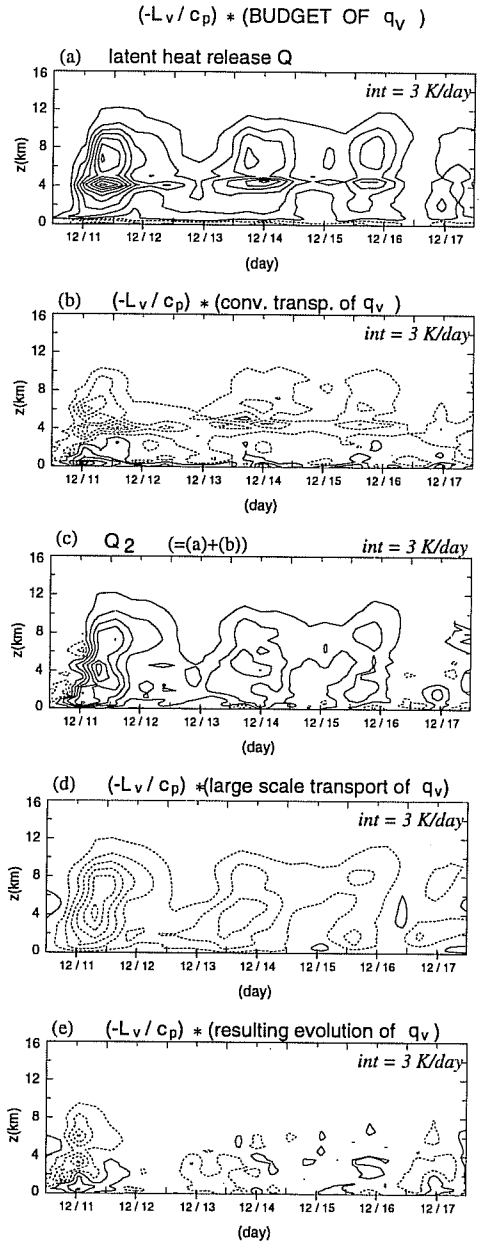

Figure 11: Evolution of different contributions to the budget of moisture sink.

Detailed discussions convective event by convective event are beyond of the scope of the present paper and will be reported later, here the evolution of different contributions to moisture budget are only shown on Fig. 11. Nevertheless, we can summarize in saying that results about the partioning of Q_1 and Q_2 reported in section 3 for a case unforced by large scale motions are broadly true for cloud systems forced by large scale motions.

If there is no major difference in the cloud-scale contributions of Q_1 and Q_2 between forced and unforced cases, a main difference is of course in term of resulting evolution of temperature and vapor. Figures. 10d and 10f show the evolution of temperature and vapor as the difference between large scale transports (as prescribed from observations) and the apparent source or sink (Q_1 and Q_2). These figures stress the difficulty to parameterize the convection in GCM as well to evaluate the convective schemes. The evolutions of vapor and of temperature are indeed very small in comparison to other terms. When looking at each individual convective events, these remarks are still true (Fig. 11).

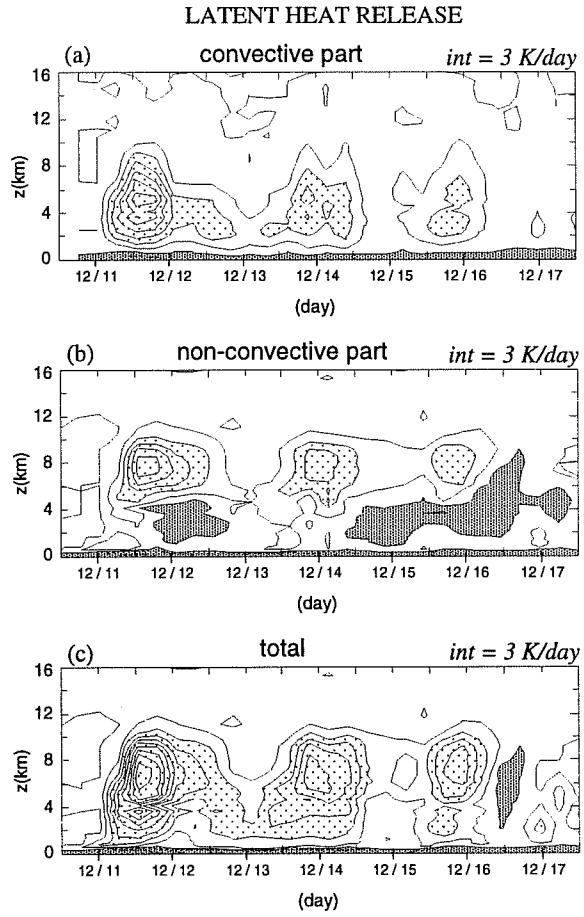

Figure 12: Evolution of the domain-averaged 6-hr mean of latent heat release $\frac{1}{\pi_0}Q^*$ (Eq. 1) (c) and contributions of convective (a) and non-convective regions (b). Dotted and hatched areas correspond to values greater than 6 K/day and negative values, respectively.

The evolution of the domain-averaged 6-hr mean of latent heat release $\frac{1}{\pi_0}Q^*$ (Eq. 1) and its partioning in convective and non-convective regions (Fig. 12) exhibit typical features observed during COPT81 (West Africa) for individual tropical convective systems (Caniaux *et al.*1994). The convective part shows a latent heat release everywhere except in the first 600 meters where the rain evaporation leads to a cooling. The stratiform region present a latent heat release above 4km, corresponding to the mean ascent occuring in stratiform region associated to tropical convective systems and a cooling below 4km, corresponding to a mean descent (Caniaux *et al.*1994). Both regions contribute to the behaviour of the total latent heat release (Fig. 12c).

A crucial quantity for mass flux convection schemes is the net mass flux. Simulations issued from cloud-resolving models are able to diagnose net mas flux as well updraft and downdraft mass fluxes. Another tool is to use Doppler radar data able to give an estimate of mass flux at least in precipitating regions. It is one of our goal to compare both estimates from Doppler radar and numerical simulations for some TOGA-COARE cases as did in the past for a squall line (Lafore *et al.*, 1988). Figure 13 illustrates the evolution of 6-hr mean of the net mass flux, the updraft and downdraft mass fluxes in the convective region (as defined in section 2). During each convective event, the vertical profile of the net mass flux (Fig. 13a) is typical, with negative values at low levels (under 1 km) and positive values above. Maxima of convective mass flux is around 4km though slightly varying as a function of the convection intensity. These maxima are clearly related to those of convective updraft mass flux (Fig. 13b). Convective downdraft mass flux (Fig. 13c) contributes

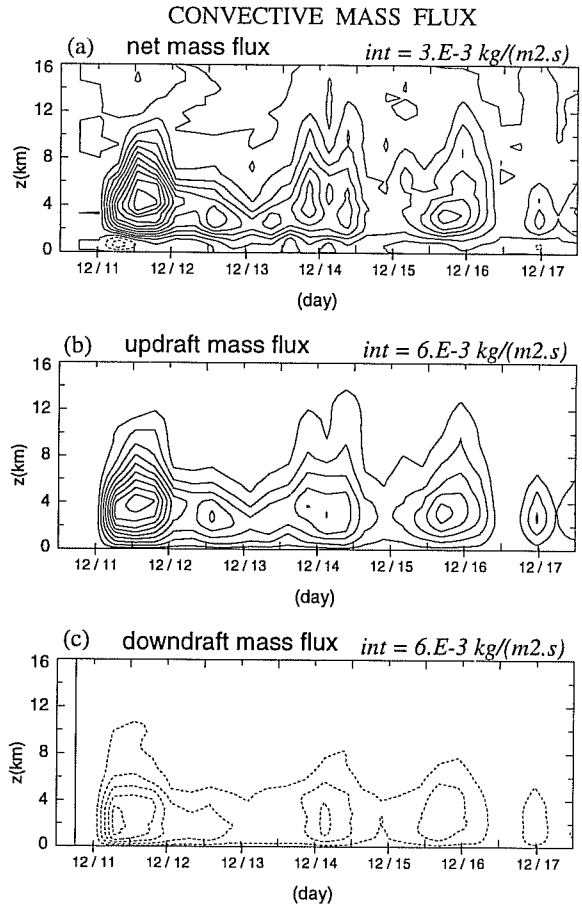

Figure 13: Evolution of the 6-hr mean of the net mass flux, the updraft and downdraft mass fluxes in the convective region (panels a, b and c, respectively).

to the net mass flux mainly at low levels and peak around 2km. As found for the 17 Feb 1993 case unforced by large scale motions, a comparison of net vertical mass fluxes and latent heat realease shows a strong correlation between these two fields. It is illustrated for the convection region by Figs. 12a and 13a.

5 CONCLUSION

The thermodynamical impact of different cloud systems observed during TOGA-COARE experiment have been investigated through detailed diagnoses issued from simulations using a cloud-resolving model. Two different approaches have been presented corresponding to different large scale flow behaviours. The first case study corresponds to the development of convective lines (17 Feb 1993), oriented approximately parallel to a moderate low level shear. This type of system is very common over the Western Equatorial Pacific, and is generally characterized by the absence of large-scale ascent. In this case, the only "external forcings" are the surface fluxes and radiative processes. The second study corresponds to larger convective systems observed during 11-18 December 1992 (before the westerly wind burst) and forced through large-scale motions. In this case, time-evolving advective effects of heat and moisture deduced from observational network are used to force the cloud-resolving model. As in the first case, surface fluxes and radiative processes are also computed at each time step of model.

Simulations of both cases have been used to compute advanced diagnostics, in order to pro-

vide new insights for development and evaluation of convective parameterizations in GCMs. The simulation domain have been partitioned into internal areas, including convective and stratiform precipitation areas as well as shallow, anvil cloud areas and clear sky columns. Also convective and stratiform region have been also partioned in updraft and downdraft regions. It is thus possible to determine from all simulations the contributions of different internal areas to the total cloud ensemble impact. Thus, from a complex cloud ensemble, we went to a simpler and more understandable system formally analogous to 1D cloud model type that are used in mass flux convection schemes.

The first case have been extensively analyzed (see also Guichard *et al.*1996b) whereas the second case is still at a first stage of analysis. Nevertheless in a broad sense, first results seem not really different between cases unforced and forced by the large scale motions.

Different behaviour of the vertical distribution of the apparent heat source Q_1 and apparent moisture sink Q_2 are obtained for all considered convcetive system. At the domain scale, differences have been explained mainly by significant convective transport of mositure, as opposed to much weaker convective transport of heat. Decomposition of budgets highlights the mechanisms of compensation occuring between the precipitating system and its environment. For temperature, the latent heat release in the precipitating part is approximately compensated by the mean vertical advection, so that the contribution of this area to the total warming is small. The total warming finally occurs mainly in the environment, through compensating subsidence. Moisture budgets are more complex to analyze, and stress the importance of lateral exchanges. In the case of 17 Feb 1993, both low level downdrafts in the precipitating system and the coexisting shallow clouds have a great impact on the budgets. For the same case, it has been shown thatconvective fluxes occur at very small scales, so that average draft profiles of vertical velocity, temperature and humidity are not enough to predict them. This result agrees with observations of convective clouds discussed by Emanuel (1991). It suggests that bulk cloud models should take into account sub-cloud scale processes. Though not shown for the 7-day simulations, in both cases (forced and unforced), in-cloud temperature excesses are weak as observed, whereas vapour excesses are significant and correlated with vertical velocity. However, buoyancy deviations are extremely small, indicating an equilibrium of density, involving thermodynamics and microphysics.

REFERENCES

Arakawa, 1. and W.H. Schubert, 1974: Interaction of a cumulus cloud ensemble with the large-scale environment, Part I, *J. Atmos. Sci.*, **31**, 674-701.

Asselin, R., 1972: Frequency filter for time integrations. *Mon. Wea. Rev.*, **100**, 487-490.

Balaji, V. and J.-L. Redelsperger, 1996: Sub-gridscale effects in mesoscale deep convection: initialisation, organization and turbulence., Review paper on "Tropospheric Turbulence" in Atmospheric Research, Vol 40/2-3.

Caniaux, G., J.–L. Redelsperger, and J.–P. Lafore, 1994a: A numerical study of the stratiform region of a fast–moving squall line. Part I: General description, and water and heat budgets. *J. Atmos. Sci.*, **51**, 2046-2074.

Emanuel, K.A., 1991: A scheme for representing cumulus convection in large-scale models, *J. Atmos. Sci.*, **48**, 2313-2335.

Grabowski, W.W., X. Wu, and M.W. Moncrieff, 1996: Cloud resolving modeling of tropical cloud systems during Phase III of GATE. Submitted to *J. Atmos. Sci.*.

Gregory, D. and M.J. Miller, 1989: A numerical study of the parametrization of deep tropical convection, *Quart. J. Roy. Meteor. Soc.*, **115**, 1209-1241.

Guichard, F., J.–L. Redelsperger and J.–P. Lafore, 1996a: The behaviour of cloud ensemble to external forcings. *Q. J. Roy. Meteor. Soc*, 122, 1043-1073.

Guichard, F., J.–P. Lafore, and J.–L. Redelsperger 1996b: Thermodynmical impact and internal structure of a cloud system. Submitted to *Q. J. Roy. Meteor. Soc.*

Jabouille, P., J.–L. Redelsperger, and J.–P. Lafore, 1996: Modification of surface fluxes by atmospheric Convection in the TOGA-COARE region. *Mon. Wea. Rev.*, **124**, 816-837.

Johnson, R.H., 1984: Partitioning tropical heat and moisture budgets into cumulus and mesoscale components: Implications for cumulus parameterization. *Mon. Wea. Rev.*, **112**, 1590–1601.

Jorgensen, D.P. and M.A. LeMone, 1989: Vertical velocity characteristics of oceanic convection, *J. Atmos. Sci.*, **46**, 621-640.

Krueger, S.K. 1988: Numerical simulation of tropical cumulus clouds and their interactions with the subcloud layer, *J. Atmos. Sci.*, **45**, 2221-2250.

Lafore, J.–P., J.–L. Redelsperger and G. Jaubert, 1988: Comparison between a three–dimensional simulation and doppler radar data of a tropical squall line: transports of mass, momentum, heat, and moisture. *J. Atmos. Sci.*, **45**, 3483–3500.

Lin, X. and R. H. Johnson, 1996: Heating, moistening and rainfall over the Western Pacific Warm Pool during TOGA-COARE, *J. Atmos. Sci.*, **November issue**, .

Lipps, F.B. and R.S. Hemler, 1986: Numerical simulation of deep tropical convection associated with large-scale convergence, *J. Atmos. Sci.*, **43**, 1796-1816.

Lucas, C., E.J. Zipser and M.A. LeMone, 1994: Vertical velocity in oceanic convection off tropical Australia, *J. Atmos. Sci.*, **51**, 3183-3193.

Morcrette, J.-J., 1991: Radiation and cloud radiative properties in the European center for medium range weather forecasts forecasting system, *J. Geophys. Res.*, **96**, 9121-9132.

Redelsperger, J.-L., and G. Sommeria, 1981: Méthode de représentation de la turbulence d'échelle inférieure à la maille pour un modèle tri-dimensionnel de convection nuageuse. *Bound.-Layer. Meteor.*, **21**, 509-530.

Redelsperger, J.-L., and G. Sommeria, 1986: Three-dimensional simulation of a convective storm: sensitivity studies on subgrid parameterizations and spatial resolutions. *J. Atmos. Sci.*, **43**, 2619-2635.

Redelsperger, J.-L., and J.-P. Lafore, 1988: A three–dimensional simulation of a tropical squall–line: Convective organization and thermodynamic vertical transport. *J. Atmos. Sci.*, **45**, 1334-1356.

Sommeria and M.A. LeMone, 1978: Direct testing of three-dimensional model of the planetary boundary layer against experimental data, *J. Atmos. Sci.*, **35**, 25-39.

Tao W.K. and J. Simpson and S.-T Soong, 1987: Statistical properties of a cloud ensemble: a numerical study, *J. Atmos. Sci.*, **44**, 3175-3187.

Tao W.K. and J. Simpson, 1989: Modeling study of a tropical squall-type convective line, *J. Atmos. Sci.*, **46**, 177-202.

Sui, C.H., K.M. Lau, W.-K. Tao and J. Simpson, 1994: The tropical water and energy cycles in a cumulus ensemble model. Part I: equilibrium climate", *J. Atmos. Sci.*, **51**, 711-728.

Tiedtke M., 1989: A comprehensive mass flux scheme for cumulus parameterization in large-scale models, *Mon. Wea. Rev.*, **117**, 1779-1800.

Yanai, M., S. Esbensen and J.-H. Chu, 1973: Determination of bulk properties of tropical cloud clusters from large-scale heat and moisture budgets, *J. Atmos. Sci.*, **30**, 611-627.